

PAPER • OPEN ACCESS

## Third-order nonlinearity with subradiance dark-state in ultra-strong excitons and surface plasmon coupling using self-antiaggregation organic dye

To cite this article: Muhammad Asif Ahmad Khushaini *et al* 2023 *Phys. Scr.* **98** 055501

View the [article online](#) for updates and enhancements.

### You may also like

- [Classifying High-cadence Microlensing Light Curves. I. Defining Features](#)  
Somayeh Khakpash, Joshua Pepper, Matthew Penny et al.
- [PROBING MILLISECOND PULSAR EMISSION GEOMETRY USING LIGHT CURVES FROM THE FERMI/LARGE AREA TELESCOPE](#)  
C. Venter, A. K. Harding and L. Guillemot
- [pyLIMA: An Open-source Package for Microlensing Modeling. I. Presentation of the Software and Analysis of Single-lens Models](#)  
E. Bachelet, M. Norbury, V. Bozza et al.



## PAPER

## OPEN ACCESS


RECEIVED  
18 August 2022REVISED  
13 December 2022ACCEPTED FOR PUBLICATION  
22 March 2023PUBLISHED  
31 March 2023

Original content from this work may be used under the terms of the [Creative Commons Attribution 4.0 licence](#).

Any further distribution of this work must maintain attribution to the author(s) and the title of the work, journal citation and DOI.



# Third-order nonlinearity with subradiance dark-state in ultra-strong excitons and surface plasmon coupling using self-antiaggregation organic dye

Muhammad Asif Ahmad Khushaini<sup>1</sup>, Nur Hidayah Azeman<sup>2</sup>, Tg Hasnan Tg Abdul Aziz<sup>1</sup>, Ahmad Ashrif A Bakar<sup>2</sup>, Richard M. De La Rue<sup>3</sup>, Ahmad Rifqi Md Zain<sup>1,\*</sup> , Burhanuddin Yeop Majlis<sup>1</sup> and Clarence Augustine TH Tee<sup>4,\*</sup>

<sup>1</sup> Institute of Microengineering and Nanoelectronics (IMEN), Universiti Kebangsaan Malaysia, 43600 UKM Bangi, Selangor, Malaysia

<sup>2</sup> Department of Electrical, Electronic and Systems Engineering, Faculty of Engineering and Built Environment, Universiti Kebangsaan Malaysia, 43600 UKM Bangi, Selangor, Malaysia

<sup>3</sup> School of Engineering, University of Glasgow, Rankine Building, Glasgow G12 8LT, United Kingdom

<sup>4</sup> College of Physics & Electrical Information Engineering, Zhejiang Normal University, Zhejiang, People's Republic of China

\* Authors to whom any correspondence should be addressed.

E-mail: [rifqi@ukm.edu.my](mailto:rifqi@ukm.edu.my) and [catht@zjnu.edu.cn](mailto:catht@zjnu.edu.cn)

**Keywords:** surface plasmon resonance, sensor, strong coupling, non-linear optics

Supplementary material for this article is available [online](#)

## Abstract

A strong coupling regime with dressed states is formed when a propagating surface plasmon (PSP) mode coherently exchanges energy with an ensemble of excitons at a rate faster than the system's losses. These states are superpositions of superradiance excitons and PSP modes, accompanied by remaining subradiance or 'dark' exciton states. Dark-states are ubiquitous, especially in disordered systems, and they rise in number as the number of excitons increases. Here, the ultra-strong coupling regime was experimentally observed with the coupling strength to bare energy as high as  $g/E_{exciton} \sim 0.23$  using a self-antiaggregation organic dye, BOBzBT<sub>2</sub> in an Otto-SPR configuration. We show that the hybrid system of excitons in a nonlinear organic dye layer and a PSP mode can be described by employing dark-state in a theory of nonlinear third-order sum-frequency generation (TSFG). Close agreement between the theory and the experiment has been demonstrated. The study opens up a new perspective for establishing a relationship between the optical properties of a third-order nonlinear material and the extent of strong coupling.

## 1. Introduction

The relative rates of the fundamental processes influence the dynamics of a collection of identical excitons confined in a cavity with a propagating surface plasmon (PSP) mode. Strong coupling is realized when the energy transfer rate between excitons and PSP mode is larger than the loss rate in the system [1, 2]. This results in the formation of an excitons-PSP hybrid with distinct eigen-energies and eigenstates, when compared with the uncoupled systems. Besides offering a fundamental understanding of light-matter interactions, the regime has distinct optical properties, allowing for major advancements in photonic computers and optical nanodevices [3].

Previously, the observations of the strong coupling were reported using a variety of organic materials. This is due to its large dipole moment which enables the observation of the strong coupling regime at room temperature [4, 5]. It is understood that an organic material with a relatively narrow absorption linewidth such as J-Aggregates is favourable to induce the strong coupling regime [6–8]. However, the self-aggregation in this sort of organic molecule appears to be a stumbling barrier in generating a repeatable resonance of the strong coupling system. This is because the aggregation caused a bathochromic shift in uncoupled material absorbance, resulting in inconsistent observation of the strong coupling response [9, 10].

Meanwhile, developing an unambiguous interpretation of the strong coupling regime has proven difficult due to several competing effects involving excitons and plasmon modes. The classical approach employs oscillators with amplitudes in Newton's equations of motion where the interaction term mediates the coupling through the coupling constant,  $g$ . On the other hand, the quantum approach to the excitons-PSP hybrid system has utilized the Tavis-Cummings (TC) model [11–13]. These studies begin by establishing a qualitative description of the dispersive behavior and the splitting, either by using a classical field or a quantized field interacting with a two-level system [14–17]. The TC model predicts the formation of an antisymmetric state for which the spontaneous emission is suppressed. This state, commonly referred to as a subradiance dark-state, is relatively long lived compared with the atomic relaxation time and maintains the original exciton energy [18, 19].

The dark-states that are delocalized across multiple molecules have been observed when disordered chromophores are strongly coupled to a cavity mode [20]. Furthermore, it is expected that the presence of semilocalized dark modes will affect coherent energy transport [21]. The exploitation of the dark-state as a theoretical foundation has proven to provide a consistent microscopic interpretation for the experimental observation [22]. Moreover, as a result of introducing the dark-state, the system can be treated as a four-level system and has been used to explain the nonlinear optical signals in the strong-coupling regime [23]. There are several studies that deal with the dark-state in nonlinear systems such as in photonic waveguides [24], electromagnetically induced transparency (EIT) [25], all-optical switching [26] - and in optomechanical systems [27]. Furthermore, it has been demonstrated that the phase matching for parametric anti-Stokes generation is self-induced due to the dark-state coherence [28].

In this study, a novel self-antiaggregation organic dye, 1,4-bis[2-(5-thiophene-2-yl)-1-benzothiophene]-2,5-dioctyloxybenzene (BOBzBT<sub>2</sub>) was employed to observe the ultra-strong coupling between excitons and PSP in an SPR-Otto experiment. The experimental result was interpreted using the theory of nonlinear third-order sum-frequency generation (TSFG), which describes the hybrid system of a collection of identical excitons in a nonlinear dielectric film and the PSP mode. The three polaritonic states including the subradiance dark-state in the TSFG model, along with the addition of phenomenological damping terms analogous to those in the density matrix formulation, enable the utilisation of the four-level system predicted in the TC model. A good theory-experiment agreement enables the prediction of the optical properties of the strong coupling regime.

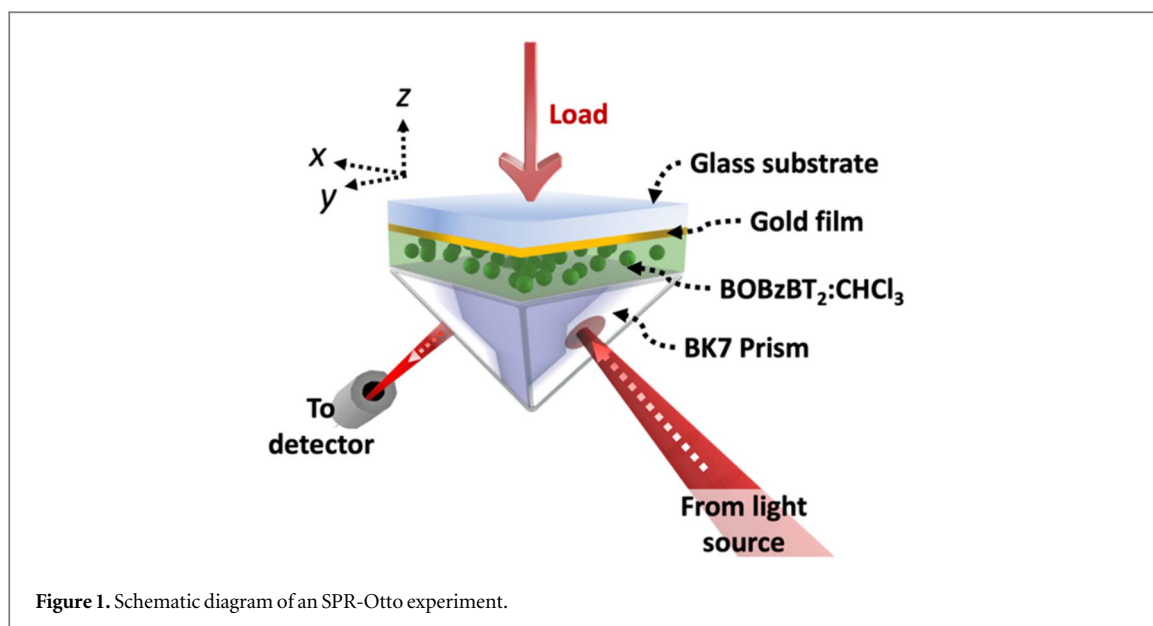
## 2. Experimental observation of the ultra-strong coupling regime

BOBzBT<sub>2</sub> was prepared according to our previous work [29] and was diluted in chloroform (CHCl<sub>3</sub>) solvent. One millilitre quantities of the dilutions with different BOBzBT<sub>2</sub>:CHCl<sub>3</sub> ratios (mg:ml) were spin-coated on to the Au film at 3,000 RPM for 40 s. Prior to that, a 50 nm thick Au layer was sputter deposited on a glass substrate using sputtering machine with the rate of 9 nm min<sup>-1</sup>. The BOBzBT<sub>2</sub> dye consists of two thiophene monomers and was added in order to enhance the nonlinear optical response [30]. The presence of bis-donor groups enhanced the efficiency of two-photon absorption [31]. The thiol groups in BOBzBT<sub>2</sub> provide for strong adhesion to the gold surface. Meanwhile, the advantages of the dioctyloxy-substituents on phenylene moiety are that the dye demonstrated good solubility in common organic solvents apart from preventing intermolecular self-aggregation [32].

A surface plasmon resonance (SPR) experiment was conducted using the Otto configuration [33]. In the Otto-SPR configuration, the sandwiched dielectric structure between metal and prism simulates an optical cavity. This facilitates the excitons-PSP coupling by reducing the energy dissipation caused by the light escaping from the system. Light was incident on the prism-dielectric layer interface with an angle,  $\theta$  and its reflectance was collected by a spectrometer. During each measurement, a drop of deionized water was placed on top of the prism before it was sandwiched with the bare Au film or the BOBzBT<sub>2</sub>:CHCl<sub>3</sub> coated Au films.

To avoid the risk of interference between the functional groups and to encourage one-to-one interaction between Frenkel excitons and PSP, deionized water is used in place of the index-matching fluid. Immersion oil, for example, has organic constituents such as the hydrogenated phenyl moiety and polybutene. Thus, using an inorganic material such as water eliminates the likelihood of interference in the strong coupling regime generated by Frenkel excitons.

The experimental setup is shown in figure 1. One of the challenges in the Otto configuration is the difficulty of adjusting the gap between the metal and the prism with precision. Several methods for controlling the gap have previously been proposed, including using a pre-defined thickness spacer coating [34], a dielectric polymer spacing layer [35], or dual-resonance fibre [36]. While using spacer foil allows for precise measurement of spacer thickness, slight differences in the thickness of the left and right spacer foils may produce inconsistent results. To achieve a relatively uniform spacer thickness, we apply a uniform load to the Au film. This is accomplished by



placing a 5 grams iron block on top of the back of Au-coated glass substrate and leaving it for 5 min to allow the excess deionized water to ooze out of the layer.

The emission and absorption spectra of BOBzBT<sub>2</sub> in CHCl<sub>3</sub> are shown in figure 2(a) where two distinct peaks are evident. Interestingly, this double-peaked spectrum is similar to the spectra of Rhodamine 6 G, an organic material that has been used to produce the strong coupling observation [14]. The frequency  $6.246 \times 10^{14}$  Hz, which correspond to the absorbance peak, has been chosen for the scaling frequency factor,  $\omega_a$  for the later experiment-theory fitting process. It was chosen because it is more pronounced than the 2.58 eV peak. In addition, 2.58 eV coincides with the emission peak. The absorbance spectra in figure 2(b) depict evidence of self-antiaggregation. In contrast to the widely employed J-aggregate and H-aggregate, neither bathochromic or hypsochromic shifts were seen when the concentration of BOBzBT<sub>2</sub> was varied.

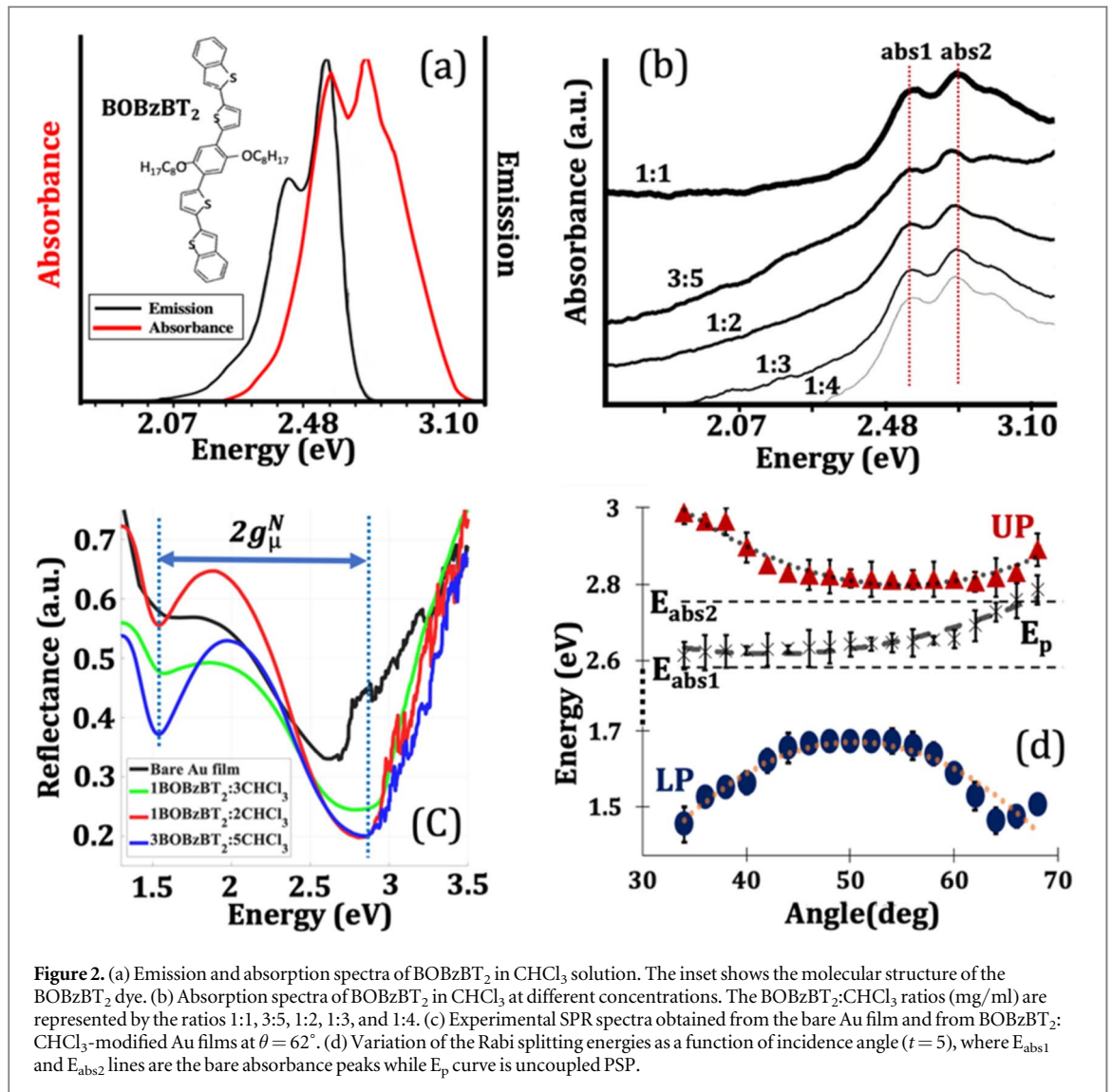
By referring to figure 2(c), it can be seen that there is only a single dip in the reflectivity curve obtained using a bare Au film at an angle of incidence of  $\theta = 62^\circ$ . However, the curve appears to have flattened between 1.5 and 2 eV. This might be attributed to increased skin depth and dissipation losses at longer wavelengths.

On the other hand, the introduction of BOBzBT<sub>2</sub> into the system, namely, by modifying Au film with 1BOBzBT<sub>2</sub>:3CHCl<sub>3</sub> dilution, resulted in the presence of a second reflectivity dip at 1.54 eV. The dip is preserved even when using a slightly higher concentration, i.e., 1BOBzBT<sub>2</sub>:2CHCl<sub>3</sub>-modified Au film. This left-hand dip becomes pronounced when the concentration of BOBzBT<sub>2</sub> is increased to 3BOBzBT<sub>2</sub>:5CHCl<sub>3</sub> implying its proportionality to the exciton number,  $N$ .

The strong coupling is characterized by the dip splitting of the SPR spectra for which the splitting width must be larger than the width of the material absorption line and the uncoupled plasmon line,  $\gamma_p$ . The linewidths of the absorbance spectrum as in figure 2(a) and the uncoupled plasmon as in figure 2(c), are determined at 560 meV and 580 meV, respectively. These values are smaller than the splitting width—with a splitting to damping ratio ( $2g/\gamma_p$ ) of  $\sim 2.1$ , which indicates that the ultra-strong coupling regime has been achieved.

In figure 2(d), the energies of the two dips representing the upper polariton (UP) and lower polariton (LP) are plotted as a function of incidence angle. The dashed lines correspond to the energies of the absorbance ( $E_{\text{abs}}$ ) and emission ( $E_{\text{emi}}$ ) lines of the uncoupled excitons while  $E_p$  represents bare PSP energies. The system exhibits very clear anti-crossing behaviour with the smallest Rabi splitting energy of  $\sim 580$  meV at an incidence angle of  $52^\circ$ . Meanwhile, the splitting energy at zero detuning value ( $E_{\text{abs}} - E_p$ ) is determined to be  $\sim 697$  meV at  $65^\circ$  of incidence angle. The error bars were calculated by taking the standard deviation for  $t = 5$ , where  $t$  is the number of repeating measurements with different 3BOBzBT<sub>2</sub>:5CHCl<sub>3</sub> coated Au films.

Many reported strong coupling experimental observations show that the upper and lower polariton dispersions asymptotically approach both the exciton and plasmon dispersions. In [37], by using two coupled harmonic oscillators, symmetrical Rabi splitting can be illustrated by equating the loss rates of both oscillators. There are, however, a number of studies where asymmetrical Rabi splitting is present [38–40]. An asymmetrical anti-crossing may be attributed to the difference in energy dissipation between material and bare cavity, or PSP mode. The discrepancy is accentuated in systems containing a disorganized ensemble of excitons, such as the one investigated herein.



### 3. Theoretical description and fitting with the experiment result

The interaction scheme for the present study is illustrated in figure 3(a). In an uncoupled system, the molecular states of the collection of excitons in a dielectric or dye film are denoted as  $|\pi\rangle$  and  $|\pi^*\rangle$ , respectively. When the light impinges on the coupling prism of an SPR setup, the strong coupling between the excitons and the PSP mode occurs. A four-level excitons-PSP hybrid system is assumed to have formed with a pair of dressed states  $|2\rangle$  and  $|4\rangle$ , together with a dark-state,  $|3\rangle$ . The dark-state is located at the same energy as the uncoupled molecular state  $|\pi^*\rangle$ . The following non-degenerate frequency components  $-\omega_1$ ,  $\omega_2$  and  $\omega_3$  are introduced to represent the transition resonance between states  $|1\rangle$ - $|2\rangle$ ,  $|2\rangle$ - $|3\rangle$  and  $|3\rangle$ - $|4\rangle$ , respectively. The hybrid system is assumed to be phase matched with the TSFG and occurs at the resonance transition between state  $|4\rangle$  and state  $|1\rangle$ . The spectral behaviour of the TSFG generated field with a frequency of  $\omega_4 = \omega_1 + \omega_2 + \omega_3$  is investigated.

To model the interaction between these frequency components, we recall the following scalar wave equation for a time-dependent electric field propagating in a nonlinear medium:

$$\nabla^2 \mathbf{E}(t) = \mu_0 \epsilon_0 (\partial^2 \mathbf{E}(t) / \partial t^2) + \mu_0 (\partial^2 \mathbf{P}^{NL}(t) / \partial t^2) \quad (1)$$

where the wave equation is obtained using the general form of Maxwell's equations in the absence of any current density or charge density.  $\mu_0$  and  $\epsilon_0$  are the permeability and permittivity of free space, respectively - while  $\mathbf{P}^{NL}$  is the induced nonlinear polarization in the medium and is expressed in terms of the field vector,  $\mathbf{E}$ .

The system is assumed to be in a phase matching condition with the following set of nonlinear polarization components, corresponding to the sum-frequency generation phenomenon:

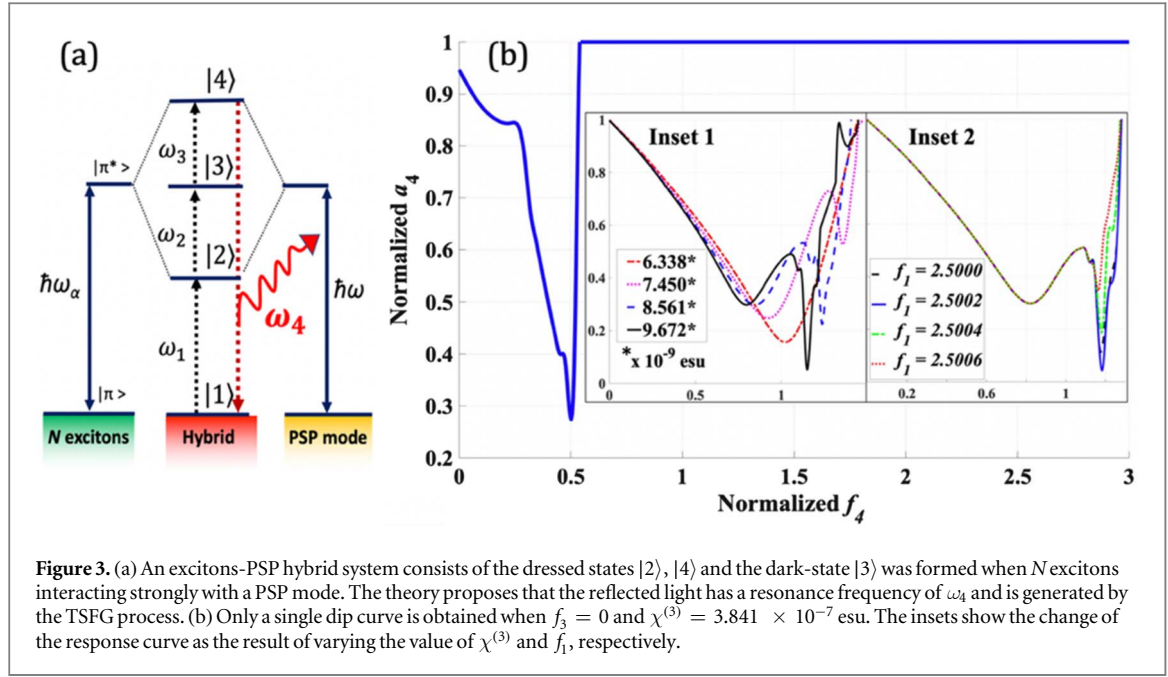


**Figure 3.** (a) An excitons-PSP hybrid system consists of the dressed states  $|2\rangle$ ,  $|4\rangle$  and the dark-state  $|3\rangle$  was formed when  $N$  excitons interacting strongly with a PSP mode. The theory proposes that the reflected light has a resonance frequency of  $\omega_4$  and is generated by the TSFG process. (b) Only a single dip curve is obtained when  $f_3 = 0$  and  $\chi^{(3)} = 3.841 \times 10^{-7}$  esu. The insets show the change of the response curve as the result of varying the value of  $\chi^{(3)}$  and  $f_1$ , respectively.

$$\begin{aligned}
 P(\omega_1 + \omega_2 + \omega_3) &= 6\epsilon_0 \chi^{(3)} E_1(t) E_2(t) E_3(t) \\
 P(\omega_2 + \omega_3 - \omega_4) &= 6\epsilon_0 \chi^{(3)} E_2(t) E_3(t) E_4^*(t) \\
 P(\omega_1 + \omega_3 - \omega_4) &= 6\epsilon_0 \chi^{(3)} E_1(t) E_3(t) E_4^*(t) \\
 P(\omega_1 + \omega_2 - \omega_4) &= 6\epsilon_0 \chi^{(3)} E_1(t) E_2(t) E_4^*(t)
 \end{aligned} \tag{2}$$

where  $\chi^{(3)}$  is the third-order nonlinear susceptibility of the medium. We have treated the field components as plane waves propagating in the  $z$ -direction. The amplitude  $E_i(t)$  assumed to be a periodic function of position that varies along the optical axis  $z$  with a period on the order of the optical wavelength  $\vec{E}_i = A_i(z)e^{ikz}$ , where  $i = 1, 2, 3, 4$ . By substituting the equation (2) into equation (1) and using the slowly-varying-amplitude-approximation,  $d^2\vec{E}_i/dz^2 \ll d\vec{E}_i/dz$ , the following set of coupled equations is obtained [41]:

$$\begin{aligned}
 \left(\frac{da_4}{du}\right) &= -if_4 \left(\frac{3}{2\pi}\right) \chi^{(3)} \vec{E}_{\min}^2 a_1 a_2 a_3 - a_4 \gamma_{41} \\
 \left(\frac{da_1}{du}\right) &= -if_1 \left(\frac{3}{2\pi}\right) \chi^{(3)} \vec{E}_{\min}^2 a_2 a_3 a_4^* - a_1 \gamma_{12} \\
 \left(\frac{da_2}{du}\right) &= -if_2 \left(\frac{3}{2\pi}\right) \chi^{(3)} \vec{E}_{\min}^2 a_1 a_3 a_4^* - a_2 \gamma_{23} \\
 \left(\frac{da_3}{du}\right) &= -if_3 \left(\frac{3}{2\pi}\right) \chi^{(3)} \vec{E}_{\min}^2 a_1 a_2 a_4^* - a_3 \gamma_{34}
 \end{aligned} \tag{3}$$

where the original equations are scaled by introducing the following dimensionless variables;  $a_i = \vec{E}_i/\vec{E}_{\min}$ ,  $u = \omega_a z/c$  and  $f_i = \omega_i/\omega_a$ —representing the scaled electric field, scaled thickness of the dielectric film and the scaled transition frequency, respectively. The value of the frequency factor  $\omega_a$  is the experimental value of the exciton resonance frequency for the uncoupled system as introduced in the previous section.  $\vec{E}_{\min}$  corresponds to the field enhancement caused by the PSP mode and is fixed at  $\vec{E}_{\min} = 10^7 \text{V m}^{-1}$ —while the field amplitude  $a_4$  can be obtained by solving equation (3) numerically. By plotting  $a_4$  against the frequency,  $f_4$ , the SPR reflectivity spectra can be observed.

Meanwhile,  $\gamma_{ij}$  ( $ij = 12, 23, 34, 41$ ) is the scaled damping parameter similar to that of phenomenological damping in density matrix formalism (more in the later section). It was included since transitions within the excitation rung of the TC model may be induced solely by emitter decay processes, such as incoherent contact with the external environment or the dipole dephasing rate attributable to processes unrelated to population transfer [42]. Moreover, in TC model, the transition to dark-state from the ground state is forbidden [43].

It is demonstrated in figure 3(b) that, with all damping parameters equal to zero and using the scaled thickness range of  $0 < u < 0.27$ , only a single dip—similar to that of the uncoupled SPR spectrum, is observed when letting  $f_3 = 0$ . On the contrary, with the nonzero  $f_3$ , the solution curve demonstrates two dips spectrum. In the experimental observations reported in [44–46], the dips are shifted as the result of changing the angle of incidence of the light. Moving the angle of incidence closer to or away from the critical angle also affects the depth of the dips.

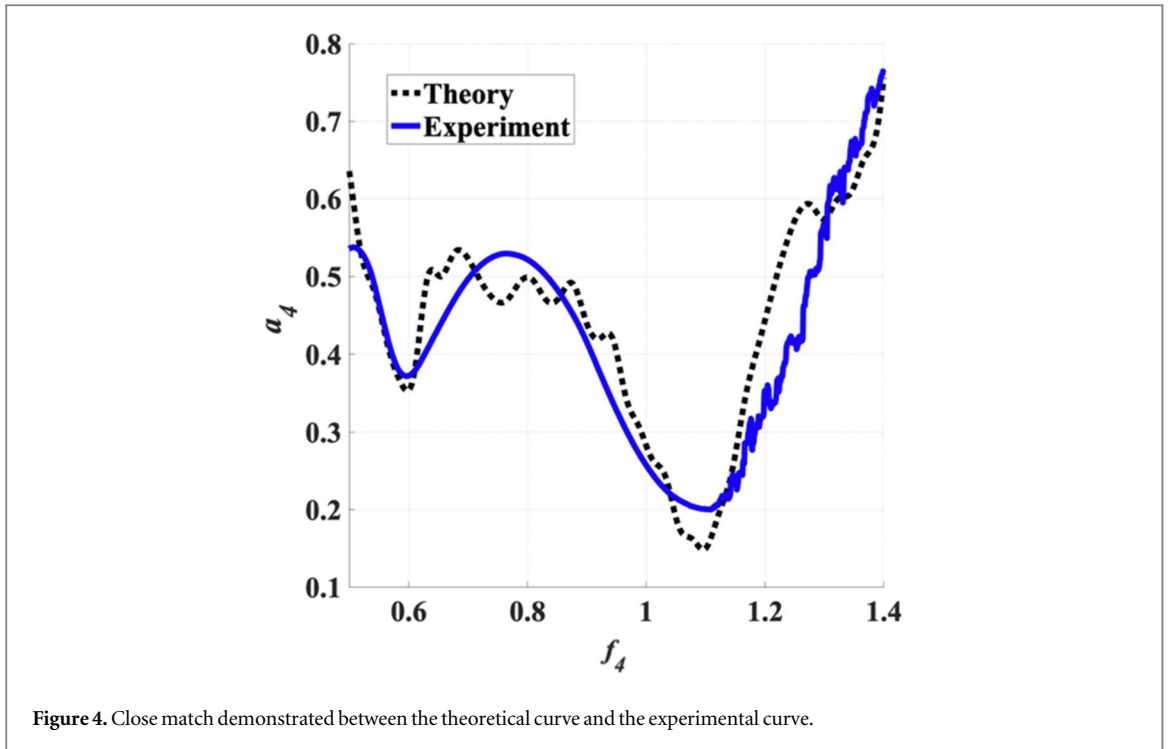


Figure 4. Close match demonstrated between the theoretical curve and the experimental curve.

By solving the equation (3) at which the value of  $\chi^{(3)}$  is increased, the aforementioned experimental observations can be closely imitated (see Inset 1 of figure 3(b)). With this similarity, we can infer that, as the incident angle approaches the critical angle, i.e., when the deflection of incident light is minimized, the strength of the evanescent wave is increased, thereby increasing the strength of  $\chi^{(3)}$  in the system. This is consistent with the fact that the large magnitude of the third-order susceptibility enhances polariton - polariton interactions [47]. In addition, the right dip is particularly sensitive to the value of  $f_1$ . As  $f_1$  increases with respect to the fixed values of  $f_2$  and  $f_3$ , the right dip diminishes and approaches a single dip SPR spectrum (see Inset 2 of figure 3(b)). This may be owing to the reasons that the separation between the dressed states  $|2\rangle$  and  $|4\rangle$  becomes smaller as  $f_1$  increases—and therefore the energy of the system approaches that of the uncoupled system.

Theoretical fitting to the experimental results was then carried out. We have used the curve obtained from the 3BOBzBT<sub>2</sub>:5CHCl<sub>3</sub> coated Au film, due to its pronounced left-hand dip - as compared with the one obtained from the 1BOBzBT<sub>2</sub>:3CHCl<sub>3</sub> and 1BOBzBT<sub>2</sub>:2CHCl<sub>3</sub> coated Au films. The energy, eV, of the  $x$ -axis on the experimental spectrum in figure 2(c) must be converted to the scaled frequency,  $f_4$ , in order to fit with the theoretical spectrum. Therefore, the experimental spectrum was scaled with the uncoupled BOBzBT<sub>2</sub> resonance frequency,  $6.246 \times 10^{14}$  Hz or 2.74 eV.

The theory showed close agreement with the experimental curve (figure 4). However, in order for the theory to match with the experimental curve, the damping terms  $\gamma_{ij}$  needed to be nonzero - namely  $\gamma_{12} = 0.429$ ,  $\gamma_{23} = 0.031$  and  $\gamma_{34} = 0.041$ . The damping for the  $|4\rangle - |1\rangle$  transition,  $\gamma_{41}$ , was fixed at  $\gamma_{41} = \gamma_{12} + \gamma_{23} + \gamma_{34}$  - while, the frequency components were set at  $f_1 = 2.500$  and  $f_2 = f_3 = 0.550$ , respectively.

#### 4. Estimation of transition dipole moment and coupling parameter

The coupling parameter for excitons-PSP hybrid can be derived by investigating the total Hamiltonian of the system. We begin by considering  $N_s$  excitons in each  $N_L$  layer - where the total Hamiltonian is given by;

$$\begin{aligned} \hat{H}_{Total} = & \sum_{j=1}^{N_L} \sum_{i=1}^{N_s} \frac{\hbar\omega_0}{2} \sigma_{i,j}^\dagger \sigma_{i,j} + \sum_{\vec{k}} \hbar\omega(\vec{k}) a_{\vec{k}}^\dagger a_{\vec{k}} \\ & + \hbar \sum_{\vec{k}} \sum_{j=1}^{N_L} \sum_{i=1}^{N_s} \frac{g_{\mu}}{\sqrt{A}} ((a_{\vec{k}} \sigma^\dagger + a_{\vec{k}} \sigma) e^{i\vec{k} \cdot \vec{r}} \\ & + (a_{\vec{k}}^\dagger \sigma + a_{\vec{k}}^\dagger \sigma^\dagger) e^{-i\vec{k} \cdot \vec{r}}) \end{aligned} \quad (4)$$

the first and second terms on the RHS of equation (4) represent the Hamiltonian for free excitons and the freely quantized PSP modes.  $\sigma_{i,j}^\dagger$  and  $\sigma_{i,j}$  are the exciton raising and lowering operators, respectively while  $a_{\vec{k}}^\dagger$  is the creation operator and  $a_{\vec{k}}$  is a destruction operator for a PSP mode. The quantization of the PSP mode is

performed by using the vector,  $u_{\vec{k}} = (L(\vec{k}))^{-1/2} e^{-\vec{k} \cdot z} (\vec{u}_{\vec{k}} + i\vec{u}_z |\vec{k}| / \vec{k}_z)$ , where the  $L(\vec{k})$  is chosen so as to normalize the energy of the mode [48].  $\vec{u}_{\vec{k}}$  and  $\vec{u}_z$  are the unit vectors for the in-plane direction ( $x$ -axis) and the vertical direction ( $z$ -axis), with respect to the in-plane momentum  $\vec{k}$  ( $z$ -axis), respectively.

The system enters the ultra-strong coupling regime when the parameter coupling,  $g$  is increased to more than 10% of the uncoupled exciton energy ( $g/E_{exciton} \gtrsim 0.1$ ) [49]. As can be seen in the experimental spectra (figure 2(c)), the system operates in the ultra-strong coupling regime with a Rabi splitting corresponding to a 23% of the uncoupled exciton energy. Thus, the interaction Hamiltonian, i.e., the third term of the RHS in equation (4) is obtained in its general form without employing the rotating wave approximation (RWA). This is due to the fact that the presence of non-negligible antiresonant light-matter coupling terms in ultra-strong coupling regime causes changes in both excited and ground state properties. However, the Hamiltonian will not be evaluated explicitly in the following analysis. Rather, the interaction term in equation (4) is used to obtain the coupling parameter expression for the case of a collection of identical excitons and the PSP mode.

$A$  is the area of the coupling site and the coupling parameter  $g_{\mu}$  can be written explicitly as  $g_{\mu} = u_{\vec{k}} \mu (\omega(\vec{k})/2\epsilon_0)^{1/2}$  where it is proportional to the value of the transition dipole moment,  $\mu$ . To approximate the total Hamiltonian as an ensemble of  $N_s \times N_L$  excitons, we define the collective mode of the  $N_s$  and  $N_L$  excitons as  $D_{j,\vec{k}}^{\dagger} = (N_s)^{-1/2} \sum_{i=1}^{N_s} (b_{i,j}^{\dagger} + b_{i,j}) e^{i\vec{k} \cdot \vec{r}}$  and  $D_{\vec{k}}^{\dagger} = (g_{\mu}^N(\vec{k}))^{-1} \sum_{j=1}^{N_L} g_{\mu} D_{j,\vec{k}}^{\dagger}$ , respectively. We assume that the system has a low pumping rate i.e.  $\sigma_{i,j}^{\dagger} \sigma_{i,j} \ll 1$  - for which we can replace the  $\sigma_{i,j}^{\dagger}$  and  $\sigma_{i,j}$  with the bosonic operators,  $b_{i,j}^{\dagger}$  and  $b_{i,j}$ , respectively [50]. This assumption is used since the experimental reflectivity dip observed has a broad linewidth (figure 2(a)), suggesting that the system is in the low excitation domain.

$g_{\mu}^N(\vec{k})$  is defined such that the collective mode operator is normalized where the summation over all  $N_L$  in the thickness  $z$  for a single mode gives (see details of the derivation in the Supplementary Information):

$$g_{\mu}^N = \sqrt{N |g_{\mu}|^2} \quad (5)$$

where,  $N = N_s N_L / Az$  is the number density, i.e. the number of excitons per unit volume.

From the theoretical-experimental fitting shown in figure 4, the value of  $\chi^{(3)}$  for 3BOBzBT<sub>2</sub>:5CHCl<sub>3</sub> is identified at  $\chi^{(3)} = 4.355 \times 10^{-7}$  esu. Third-order nonlinearity in strong coupling systems is not unique. There were previous research reports on strong-coupling observations using organic materials with relatively high third-order susceptibility values, such as polymethine dye, Rhodamine 6 G, and P3HT [51, 52]. To estimate the value of the transition dipole moment,  $\mu_{41}$  for 3BOBzBT<sub>2</sub>:5CHCl<sub>3</sub> and subsequently, the value of coupling constant,  $g_{\mu_{41}}^N$ , a quantum mechanical description of  $\chi^{(3)}$  must be employed. This description uses the density matrix formulation - which is more appropriate in the circumstances where there is an ensemble of identical excitons. Moreover, the formulation permits the addition of the phenomenological damping,  $\gamma_{ij}$  which rationalize the transition between polaritonic states as utilized in the present theory. The density matrix expression for  $\mu_{41}$  is given by [53, 54];

$$\mu_{41}^4 = N \hbar^3 \chi^{(3)} \gamma_{12}^2 \times \left[ \frac{((\gamma_{12} + \gamma_{23}) \omega_a (f_4 - f_{123}))^2 + (i\gamma_{41}(\gamma_{12} + \gamma_{23}))^2}{-\gamma_{12}(\gamma_{12} + \gamma_{23}) \omega_a (f_4 - f_{123}) - i\gamma_{41} \gamma_{12}(\gamma_{12} + \gamma_{23})} \right] \quad (6)$$

where  $f_{123} = f_1 + f_2 + f_3$  and at the resonance,  $f_4 - f_{123} = 0$ . In the following estimation of  $\mu_{41}$ , we choose the number density at  $N = 8.7 \times 10^{26} \text{ m}^{-3}$ . This choice is made considering that the molecular weight of BOBzBT<sub>2</sub> is higher than that of the TDBC molecule - for which a value of  $N = 1.47 \times 10^{25} \text{ m}^{-3}$  was obtained in [55]. By using the value of  $\chi^{(3)}$  obtained from fitting process, we estimate that the value of the transition dipole moment is  $\mu_{41} = 2.365 \text{ D}$ . Substituting  $\mu_{41}$  into equation (6) and observing the change of  $\chi^{(3)}$  with respect to  $f_4$  reveals that the resonance frequency of the strong coupling regime is  $f_4 = 3.599$ , (see figure 5(a)). While the magnitude of  $\chi^{(3)}$  depends on the value of  $\mu_{41}$ ,  $N$  and  $\gamma_{ij}$  - varying the frequency components in equation (6) shifts the resonance as demonstrated in the inset of figure 5(a).

Following the estimation of  $\mu_{41}$ , the behavior of the coupling constant  $g_{\mu_{41}}^N$  with respect to  $f_4$  is investigated.

Here, only the vector perpendicular to  $\vec{k}$ , i.e.  $i\vec{u}_z |\vec{k}| / \vec{k}_z$  in equation (5), is considered - since the coupling strength is at its highest value when the molecular orientation is perpendicular to the cavity surface [56]. To calculate the value of  $L(\vec{k})$ , the value of the dielectric function for the Au film is estimated using the Drude-Sommerfeld dynamical equation for a free-electron with the following bulk Au values of the plasma frequency,  $\omega_p = 13.8 \times 10^{15} \text{ s}^{-1}$  and the damping term,  $\Gamma = 1.075 \times 10^{14} \text{ s}^{-1}$ , respectively [57, 58]. To estimate the thickness of the dielectric layer, we have carried out a theoretical calculation using linear Fresnel analysis at both the dielectric-prism and the dielectric-Au layer interfaces - and have fitted it to the experimental results in figure 2(c). At  $z = 130 \text{ nm}$ , the theoretical curves match with the experimental dips. However, as the linear



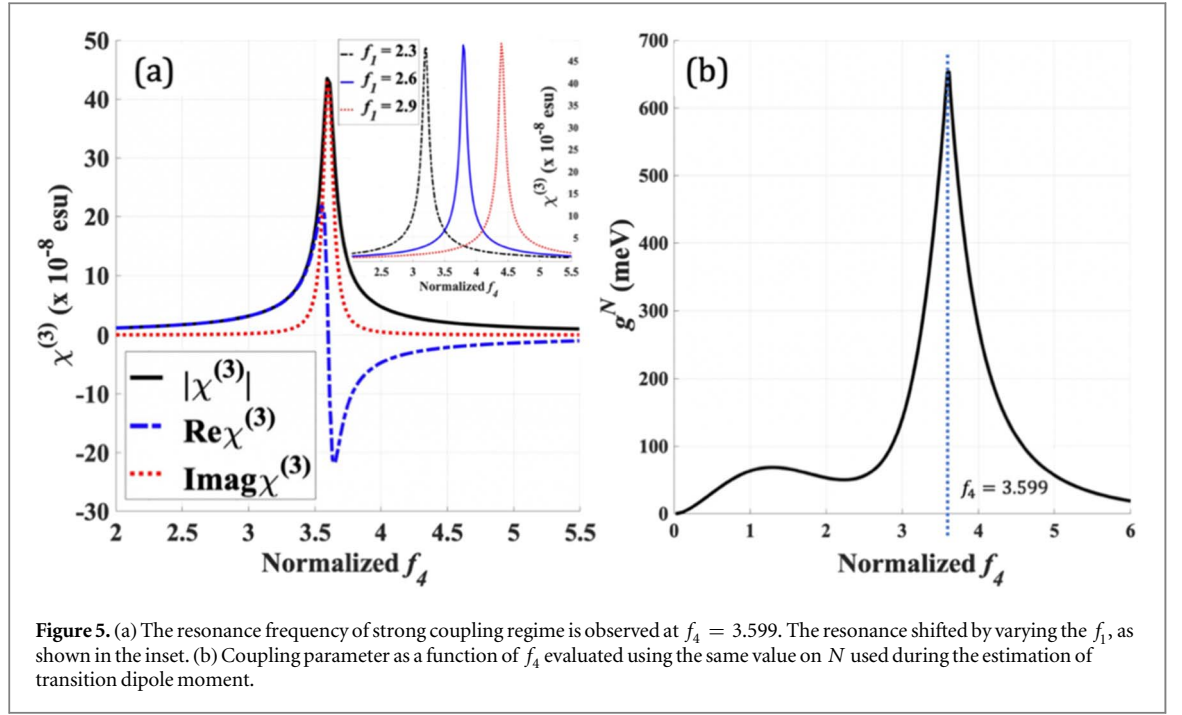


**Figure 5.** (a) The resonance frequency of strong coupling regime is observed at  $f_4 = 3.599$ . The resonance shifted by varying the  $f_1$ , as shown in the inset. (b) Coupling parameter as a function of  $f_4$  evaluated using the same value on  $N$  used during the estimation of transition dipole moment.

optics treatment failed to predict the dynamics of strong coupling, two distinct values of dielectric constant,  $\epsilon_2$  were used to fit the left and right dips namely  $\epsilon_2 = 49.3 + 28.1i$  and  $\epsilon_2 = 35.0 + 36.2i$ , respectively.

The experimental coupling parameter value,  $g_\mu^N = 659$  meV (figure 2(c)) can be obtained by evaluating equation (5) using the same number density value,  $N = 8.7 \times 10^{26} \text{ m}^{-3}$ , and the thickness of the dielectric layer,  $z = 130$  nm as demonstrated in figure 5(b). However, to obtain the same resonance frequency at  $f_4 = 3.599$  as in figure 5(a), the dielectric function must be equal to  $\epsilon_2 = 46.3 + 28.1i$ , which is between the values of  $\epsilon_2$  estimated using a linear optics formalism. Furthermore, this value of  $\epsilon_2$  is near the dielectric constant value of dimethyl sulfoxide (DMSO)  $(\text{CH}_3)_2\text{SO}$ , another well-known organosulfur compound [59].

## 5. Comparison with dressed state formalism

Previous theoretical work that deals with the strong coupling regime has mainly been developed by employing the two-level dressed state formalism. While the two-level system is useful in describing the splitting, only a qualitative description can be deduced from the models [60]. On the contrary, the TSFG theory proposed in the present work offers a unique combination from the viewpoint of the interaction between the energy levels and the nonlinear optical response. To compare, we investigate the system in figure 3(a) for an avoided crossing between the dressed states  $|2\rangle$  and  $|4\rangle$ —but this time, by excluding the dark-state,  $|3\rangle$ .

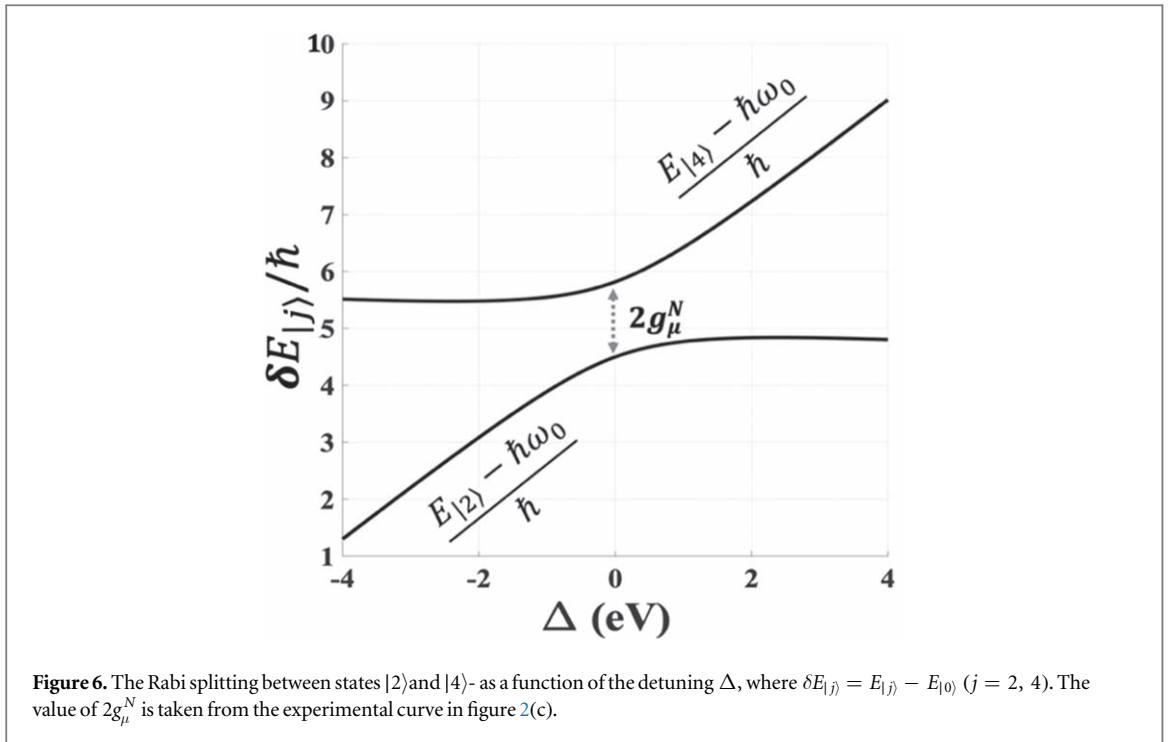
A tensor product from two Hilbert spaces, namely  $|n\rangle \otimes |i\rangle = |n, i\rangle$  where  $|n\rangle$  and  $|i\rangle$  represent the photon state at photon number  $n$  and the  $i^{\text{th}}$  exciton state, respectively were considered. We start with a diagonalization of the following  $2 \times 2$  Hermitian matrix;

$$\hat{H}^{(n)} = \hbar \begin{bmatrix} n\omega - \omega_0/2 & ig_\mu^N \sqrt{n} \\ -ig_\mu^N \sqrt{n} & (n-1)\omega + \omega_0/2 \end{bmatrix} \quad (7)$$

by using the rotation matrix,  $R(\theta)$ , and the eigenvalue matrix,  $S$ - i.e.  $\hat{H}^{(n)} = R(\theta)SR(\theta)^{-1}$ . The characteristic polynomial for the determinant of the matrix  $\hat{H}^{(n)}$  i.e.  $E_\pm = (x_1 - x_2 \pm \sqrt{(x_1 - x_2)^2 + 4x_3^2})/2$  has also been employed, where we let  $n\omega - \omega_0/2 = x_1$ ,  $(n-1)\omega + \omega_0/2 = x_2$  and  $ig_\mu^N \sqrt{n} = x_3$ . Subsequently, the expression of eigen-energies for a pair of dressed states  $|2\rangle$  and  $|4\rangle$  is given by (a detailed account of its derivation is presented in the Supplementary Information):

$$E_{|4\rangle,|2\rangle} = (n-0.5)\omega \pm 0.5\hbar\Omega_n \quad (8)$$

$\Omega_n = (\Delta^2 + 4ng_\mu^N)^{1/2}$  is the generalized Rabi frequency and  $\Delta$  is the detuning frequency, namely  $\Delta = \omega - \omega_0$  where  $\omega_0$  is the excitons-PSP resonance frequency. By letting  $n = 1$ , we plot  $\delta E_{|4\rangle}/\hbar$  and  $\delta E_{|2\rangle}/\hbar$  as a function of  $\Delta$  where at  $\Delta = 0$ , the values of the eigen-energies for the dressed states  $|2\rangle$  and  $|4\rangle$  can be



expressed as  $E_{|2\rangle} = (4.498 + \omega_0)\hbar$  and  $E_{|4\rangle} = (5.817 + \omega_0)\hbar$ , respectively (figure 6). By using equation (8) and substituting  $g_{\mu}^N = 659$  meV into  $\Omega_n$ ,  $\omega_0$  is calculated to be:  $\omega_0 = 2.494 \times 10^{15}$  Hz.

Meanwhile, the TSFG resonance predicted by the theoretical fitting to the experimental results is determined to be:  $f_4 = 3.599$ . Since  $f_4 = \omega_4/\omega_n$ , the value of  $\omega_4$ , which also represents the excitons-PSP resonance frequency, is determined at  $\omega_4 = 2.246 \times 10^{15}$  Hz.

It can therefore be seen that the difference between the excitons-PSP hybrid resonance,  $\omega_0$ , calculated via the dressed state formalism with experimental coupling parameter,  $g_{\mu}^N$ , and  $\omega_4$ , predicted by the theory of TSFG, is  $\approx 1$  eV which is coincide with the value of Frenkel exciton binding energy. Furthermore, this disparity is owing to the fact that when calculating equation (8), only a single exciton is considered. The theory of TSFG, on the other hand, was constructed based on the presence of the dark-state in the system. This, as anticipated in the Otto-SPR configuration, implies that the system contains many excitons, because the number of dark-states grows as the number of excitons increases [20].

## 6. Conclusions

In summary, we report the experimental observation of ultra-strong exciton-PSP coupling in an SPR system using the Otto configuration. The large Rabi splitting corresponding to 23% of the uncoupled exciton energy is obtained using an organic dye, BOBzBT<sub>2</sub>. BOBzBT<sub>2</sub> has self-antiaggregation properties, which permits the construction of a stable strong coupling system even in a relatively exposed configuration like the SPR setup. We demonstrated, for the first time, that the values of the transition dipole moment and coupling parameter in the strong coupling regime can be estimated analytically by combining the third-order nonlinearity theory of sum-frequency generation (TSFG) with the subradiance dark-state predicted in the TC model. The theory also consistently responds to the behaviour of a strong coupling system, and the good fit with the experimental results confirms the applicability of our model. To test the proposed theory, we compared it to the existing dressed state formalism and found that the difference in excitons-PSP resonance frequency is  $\sim 1$  eV, which corresponds to the Frenkel binding energy. Aside from emphasising the significance of self-antiaggregation dye in strong coupling systems and allowing for a practical implementation of the subradiance dark-state to describe the phenomenon, present work paves the way for the discovery of a previously unknown link between optical characteristics in the strong coupling regime.

## Acknowledgments

This work was financially supported by the Ministry of Higher Education (MoHE) of Malaysia through fundamental research grant initiative (grant numbers FRGS/1/2022/STG05/UKM/02/4)

## Data availability statement

All data that support the findings of this study are included within the article (and any supplementary files).

## ORCID iDs

Ahmad Rifqi Md Zain  <https://orcid.org/0000-0002-4611-341X>

## References

- [1] Cao E, Lin W, Sun M, Liang W and Song Y 2018 Exciton-plasmon coupling interactions: from principle to applications *Nanophotonics* **7** 145–67
- [2] Khushaini M A A, Azeman N H, Mat Salleh M, Tg Abdul Aziz T H, Bakar A, A A, De La Rue R M and Md Zain A R 2022 Exploiting a strong coupling regime of organic pentamer surface plasmon resonance based on the Otto configuration for creatinine detection *Opt. Express* **30** 14478
- [3] Sukharev M and Pachter R 2018 Effects of exciton-plasmon strong coupling on third harmonic generation by two-dimensional WS<sub>2</sub> at periodic plasmonic interfaces *J. Chem. Phys.* **148** 094701
- [4] Feist J, Galego J and Garcia-Vidal F J 2018 Polaritonic chemistry with organic molecules *ACS Photonics* **5** 205–16
- [5] Kéna-Cohen S, Maier S A and Bradley D D C 2013 Ultrastrongly coupled exciton-polaritons in metal-clad organic semiconductor microcavities *Adv. Opt. Mater.* **1** 827–33
- [6] Sorokin A V, Ropakova I Y, Grynyov R S, Vilksky M M, Liakh V M, Borovoy I A, Yefimova S L and Malyukin Y V 2018 Strong difference between optical properties and morphologies for J-Aggregates of similar cyanine dyes *Dyes Pigm.* **152** 49–53
- [7] Dintinger J, Klein S, Bustos F, Barnes W L and Ebbesen T W 2005 Strong coupling between surface plasmon-polaritons and organic molecules in subwavelength hole arrays *Physical Review B* **71** 035424
- [8] Sugawara Y, Kelf T A, Baumberg J J, Abdelsalam M E and Bartlett P N 2006 Strong coupling between localized plasmons and organic excitons in metal nanovoids *Phys. Rev. Lett.* **97** 266808
- [9] Zengin G, Johansson G, Johansson P, Antosiewicz T J, Käll M and Shegai T 2013 Approaching the strong coupling limit in single plasmonic nanorods interacting with J-aggregates *Sci. Rep.* **3** 3074
- [10] Czikkely V, Forsterling H D and Kuhn H 1970 Extended dipole model for aggregates of dye molecules *Chem. Phys. Lett.* **6** 207–10
- [11] Fink J M, Göppl M, Baur M, Bianchetti R, Leek P J, Blais A and Wallraff A 2008 Climbing the Jaynes-Cummings ladder and observing its nonlinearity in a cavity QED system *Nature* **454** 315–8
- [12] Kasprzak J, Reitzenstein S, Muljarov E A, Kistner C, Schneider C, Strauss M, Höfling S, Forchel A and Langbein W 2010 Up on the Jaynes-Cummings ladder of a quantum-dot/microcavity system *Nat. Mater.* **9** 304–8
- [13] Tavis M and Cummings F W 1968 Exact solution for an n -molecule—Radiation-field hamiltonian *Phys. Rev.* **170** 379–84
- [14] Törmä P and Barnes W L 2015 Strong coupling between surface plasmon polaritons and emitters: a review *Rep. Prog. Phys.* **78** 013901
- [15] Sáez-Blázquez R, Feist J, Fernández-Domínguez A I and García-Vidal F J 2017 Enhancing photon correlations through plasmonic strong coupling *Optica* **4** 1363
- [16] Neuman T and Aizpurua J 2018 Origin of the asymmetric light emission from molecular exciton-polaritons *Optica* **5** 1247
- [17] Herrera F and Spano F C 2018 Theory of nanoscale organic cavities: the essential role of vibration-photon dressed states *ACS Photonics* **5** 65–79
- [18] Bienaimé T, Piovela N and Kaiser R 2012 Controlled dicke subradiance from a large cloud of two-level systems *Phys. Rev. Lett.* **108** 123602
- [19] Ribeiro R F, Martínez-Martínez L A, Du M, Campos-Gonzalez-Angulo J and Yuen-Zhou 2018 Polariton chemistry: controlling molecular dynamics with optical cavities *J. Chem. Sci.* **9** 6325–39
- [20] Botzung T, Hagenmüller D, Schütz S, Dubail J, Pupillo G and Schachenmayer J 2020 Dark state semilocalization of quantum emitters in a cavity *Physical Review B* **102** 144202
- [21] Chávez N C, Mattiotti F, Méndez-Bermúdez J A, Borgonovi F and Celardo G L 2021 Disorder-enhanced and disorder-independent transport with long-range hopping: Application to molecular chains in optical cavities *Phys. Rev. Lett.* **126** 153201
- [22] Herrera F and Spano F C 2017 Dark vibronic polaritons and the spectroscopy of organic microcavities *Phys. Rev. Lett.* **118** 223601
- [23] Herrera F, Peropadre B, Pachon L A, Saikin S K and Aspuru-Guzik A 2014 Quantum nonlinear optics with polar J-aggregates in microcavities *The Journal of Physical Chemistry Letters* **5** 3708–15
- [24] Wang Z, Jaako T, Kirton P and Rabl P 2020 Supercorrelated radiance in nonlinear photonic waveguides *Phys. Rev. Lett.* **124** 213601
- [25] Yelin S F, Sautenkov V A, Kash M M, Welch G R and Lukin M D 2003 Nonlinear optics via double dark resonances *Phys. Rev. A* **68** 063801
- [26] Scheuer J, Sukhorukov A A and Kivshar Y S 2010 All-optical switching of dark states in nonlinear coupled microring resonators *Opt. Lett.* **35** 3712
- [27] Huang Y-X, Zhou X-F, Guo G-C and Zhang Y-S 2015 Dark state in a nonlinear optomechanical system with quadratic coupling *Phys. Rev. A* **92** 013829
- [28] Hakuta K, Katsuragawa M and Suzuki M 1997 1733 Dark-state coherence and stimulated Raman scattering in solid hydrogen *Philos. Trans. R. Soc. London, Ser. A* **355** 2405–8
- [29] Khushaini M A A, Azeman N H, Ismail A G, Teh C-H, Salleh M M, Bakar A A A, Aziz T H T A and Zain A R M 2021 High stability resistive switching mechanism of a screen-printed electrode based on BOBZBT2 organic pentamer for creatinine detection *Sci. Rep.* **11** 23519
- [30] Norman P, Cronstrand P and Ericsson J 2002 Theoretical study of linear and nonlinear absorption in platinum-organic compounds *Chem. Phys.* **285** 207–20
- [31] Cronstrand P, Luo Y and Ågren H 2002 Effects of dipole alignment and channel interference on two-photon absorption cross sections of two-dimensional charge-transfer systems *J. Chem. Phys.* **117** 11102–6
- [32] Khushaini M A A et al 2022 Electrochemical metallization process on screen-printed electrode for creatinine monitoring application *IEEE Sens. J.* **22** 9268–75

- [33] Otto A 1968 Excitation of nonradiative surface plasma waves in silver by the method of frustrated total reflection *Zeitschrift Für Physik A Hadrons and Nuclei* **216** 398–410
- [34] Fontana E, Kim J-M, Llamas-Garro I and Cavalcanti G O 2015 Microfabricated Otto chip device for surface plasmon resonance-based optical sensing *Appl. Opt.* **54** 9200
- [35] Srivastava T, Purkayastha A and Jha R 2016 Graphene based surface plasmon resonance gas sensor for terahertz *Opt. Quantum Electron.* **48** 334
- [36] Li L, Liang Y, Guang J, Cui W, Zhang X, Masson J-F and Peng W 2017 Dual Kretschmann and Otto configuration fiber surface plasmon resonance biosensor *Opt. Express* **25** 26950
- [37] Rodriguez S R-K 2016 Classical and quantum distinctions between weak and strong coupling *Eur. J. Phys.* **37** 025802
- [38] Hou S, Qu Y, Liu X and Forrest S R 2019 Ultrastrong coupling of vibrationally dressed organic Frenkel excitons with Bloch surface waves in a one-sided all-dielectric structure *Physical Review B* **100** 045410
- [39] Held M, Graf A, Zakharko Y, Chao P, Tropf L, Gather M C and Zaumseil J 2018 Ultrastrong coupling of electrically pumped near-infrared exciton-polaritons in high mobility polymers *Adv. Opt. Mater.* **6** 1700962
- [40] Yu Y, Mallick S, Wang M and Börjesson K 2021 Barrier-free reverse-intersystem crossing in organic molecules by strong light–matter coupling *Nat. Commun.* **12** 3255
- [41] Khushaini M A A and Ibrahim A-B M A 2016 On the optical bistability of ferroelectrics via two-wave mixing: beyond the slowly varying envelope approximation *Opt. Commun.* **381** 384–90
- [42] Gunderman L G, Stasiuk A, Mandouh M E, Borneman T W and Cory D G 2022a Lamb shift statistics in mesoscopic quantum ensembles *Quantum Inf. Process.* **21** 26
- [43] DelPo C A, Kudisch B, Park K H, Khan S-U-Z, Fassioli F, Fausti D, Rand B P and Scholes G D 2020 Polariton transitions in femtosecond transient absorption studies of ultrastrong light–molecule coupling *The Journal of Physical Chemistry Letters* **11** 2667–74
- [44] Memmi H, Benson O, Sadofev S and Kalusniak S 2017 Strong coupling between surface plasmon polaritons and molecular vibrations *Phys. Rev. Lett.* **118** 126802
- [45] Bellessa J, Bonnand C, Plenet J C and Mugnier J 2004 Strong coupling between surface plasmons and excitons in an organic semiconductor *Phys. Rev. Lett.* **93** 036404
- [46] Xu X and Jin S 2020 Strong coupling of single quantum dots with low-refractive-index/high-refractive-index materials at room temperature *Sci. Adv.* **6** 1–9
- [47] Barachati F, Simon J, Getmanenko Y A, Barlow S, Marder S R and Kéna-Cohen S 2018 Tunable third-harmonic generation from polaritons in the ultrastrong coupling regime *ACS Photonics* **5** 119–25
- [48] Archambault A, Marquier F, Greffet J-J and Arnold C 2010 Quantum theory of spontaneous and stimulated emission of surface plasmons *Physical Review B* **82** 035411
- [49] Forn-Díaz P, Lamata L, Rico E, Kono J and Solano E 2019 Ultrastrong coupling regimes of light–matter interaction *Rev. Mod. Phys.* **91** 025005
- [50] González-Tudela A, Huidobro P A, Martín-Moreno L, Tejedor C and García-Vidal F J 2013 Theory of strong coupling between quantum emitters and propagating surface plasmons *Phys. Rev. Lett.* **110** 126801
- [51] Wang H et al 2016 Dynamics of strong coupling between j-aggregates and surface plasmon polaritons in subwavelength hole arrays *Adv. Funct. Mater.* **26** 6198–205
- [52] Peters V N, Faruk M O, Asane J, Alexander R, Peters D A, Prayakarao S, Rout S and Noginov M A 2019 Effect of strong coupling on photodegradation of the semiconducting polymer P3HT *Optica* **6** 318
- [53] Boyd R W 2008 *Nonlinear Optics* (New York: Academic) 3rd ed
- [54] Buckingham A D and Fischer P 2000 Phenomenological damping in optical response tensors *Phys. Rev. A* **61** 035801
- [55] Gentile M J, Horsley S A R and Barnes W L 2016 Localized exciton-polariton modes in dye-doped nanospheres: a quantum approach *J. Opt.* **18** 015001
- [56] Berghuis A M, Serpenti V, Ramezani M, Wang S and Gómez Rivas J 2020 Light–matter coupling strength controlled by the orientation of organic crystals in plasmonic cavities *The Journal of Physical Chemistry C* **124** 12030–8
- [57] Derkachova A, Kolwas K and Demchenko I 2016 Dielectric function for gold in plasmonics applications: size dependence of plasmon resonance frequencies and damping rates for nanospheres *Plasmonics* **11** 941–51
- [58] Johnson P B and Christy R W 1972 Optical constants of the noble metals *Physical Review B* **6** 4370–9
- [59] O’Neil M J, Heckelman P E, Dobbelaar P H, Roman K J, Kenny C M and Karaffa L S (ed) 2013 (Royal Society of Chemistry) p. 593
- [60] Kenfack-Sadem C, Ekengoue C M, Danga J E, Fotue A J, Fobasso M F C and Fai L C 2020 Laser control of polariton using Landau–Zener–Stückelberg interferometry theory *The European Physical Journal Plus* **135** 815